Article

$Na_{1+y}VPO_4F_{1+y}$ ($0 \leq y \leq 0.5$) as Cathode Materials for Hybrid Na/Li Batteries

Nina V. Kosova * and Daria O. Rezepova

Institute of Solid State Chemistry and Mechanochemistry SB RAS, 18 Kutateladze, Novosibirsk 630128, Russia; rezepova_do@yahoo.com

* Correspondence: kosova@solid.nsc.ru; Tel.: +7-383-233-2410 (ext. 1115)

Abstract: Using Rietveld-refined X-ray diffraction (XRD), Fourier transform infrared spectroscopy (FTIR) and electrochemical cycling, it was established that among sodium vanadium fluorophosphate compositions $Na_{1+y}VPO_4F_{1+y}$ ($0 \leq y \leq 0.75$), the single-phase material $Na_{1.5}VPO_4F_{1.5}$ or $Na_3V_2(PO_4)_2F_3$ with a tetragonal structure (the $P4_2/mnm$ S.G.) is formed only for $y = 0.5$. The samples with $y < 0.5$ and $y > 0.5$ possessed different impurity phases. $Na_3V_2(PO_4)_2F_3$ could be considered as a multifunctional cathode material for the fabrication of lithium-ion and sodium-ion high-energy batteries. The reversible discharge capacity of 116 mAh·g^{-1} was achieved upon cycling $Na_3V_2(PO_4)_2F_3$ in a hybrid Na/Li cell. Decrease in discharge capacity for the other samples was in accordance with the amount of the electrochemically active phase $Na_3V_2(PO_4)_2F_3$. $Na_3V_2(PO_4)_2F_3$ showed good cycleability and a high rate of performance, presumably due to operation in the mixed Na/Li electrolyte. The study of the structure and composition of charged and discharged samples, and the analysis of differential capacity curves showed a negligible Na/Li electrochemical exchange, and a predominant sodium-based cathode reaction. To increase the degree of the Na/Li electrochemical exchange in $Na_3V_2(PO_4)_2F_3$, it needs to be desodiated first in a Na cell, and then cycled in a lithium cell. In this case, the electrolyte would be enriched with the Li ions.

Keywords: $Na_3V_2(PO_4)_2F_3$; $NaVPO_4F$; XRD; hybrid Na/Li batteries

1. Introduction

In recent years, investigations in the energy saving field have focused on the development of sodium-ion batteries, as sodium is much more abundant, ecologically sound, and cheaper than lithium [1]. The main issue for Na-ion based systems is their lower energy density compared to the Li-ion systems, and the smaller choice of electrode materials available for sodium technology. There has been significant interest in polyanion-based active cathode materials as safer alternatives to traditional oxide cathodes [2]. Among them, vanadium-based polyanion compounds such as sodium vanadium phosphate and sodium vanadium fluorophosphates have attracted great attention because of their high operating potential based on the inductive effects of both PO_4^{3-} and F^- anions, and high expected specific capacity due to the multiple accessible oxidation states of vanadium. Sodium vanadium fluorophosphates show higher energy density than $Na_3V_2(PO_4)_3$, owing to the substitution of one PO_4^{3-} group for F^- in the structure, leading to an increase in the sodium ion insertion voltage.

With respect to sodium–vanadium fluorophosphates, three phases are described in the literature: $NaVPO_4F$, $Na_3(VO)_2(PO_4)_2F$ and $Na_3V_2(PO_4)_2F_3$. $NaVPO_4F$ was first proposed as a cathode material by Barker et al. in 2003 [3]. Its theoretical specific capacity, assuming the reversible intercalation of one Na^+ ion per formula unit (f.u.), amounts to 143 mAh·g^{-1}. It is reported that $NaVPO_4F$ exists in two polymorphs: the low-temperature monoclinic phase (S.G. $C2/c$), and the high-temperature tetragonal phase (S.G. $I4/mmm$) [4]. Tetragonal $NaVPO_4F$ is structurally related to the known Na-ion

conductor, α-Na$_3$Al$_2$(PO$_4$)$_2$F$_3$ [5], and possesses the lattice parameters $a = b = 6.387$ Å and $c = 10.734$ Å. However, some additional peaks can be found on the XRD patterns of NaVPO$_4$F when prepared by the ceramic method [3]. The presence of Na$_3$V$_2$(PO$_4$)$_3$ or other impurities is possible because sublimation of VF$_3$ can occur at high temperatures.

Sauvage et al. [6] found the "NaVPO$_4$F" stoichiometry based on a single structural consideration rather suspicious. They re-investigated the system, tuning the synthesis conditions previously reported by Barker et al. [3], and obtained a single-phase material assigned to Na$_{1.5}$VOPO$_4$F$_{0.5}$ crystallized in the $I4/mmm$ S.G. Recently, Tsirlin et al. [7] have proposed the $P42/mnm$ S.G. for the room temperature phase among various polymorphs of this material at different temperatures. Actually, Na$_{1.5}$VOPO$_4$F$_{0.5}$ or Na$_3$(VO)$_2$(PO$_4$)$_2$F belongs to a family of the mixed-valence sodium vanadium fluorophosphates Na$_3$V$_2$O$_{2y}$(PO$_4$)$_2$F$_{3-2y}$ ($0 \leq y \leq 1$). These materials have a similar tetragonal structure, but differ by the amount of the F$^-$ atoms replaced by O^{2-} in the 8j positions and the oxidation state of the V ions, which varies between 3+ and 4+, with a concomitant modification of the physical and electrochemical properties of the material [8–11]. Depending on y, the average voltage of the cell varies from 3.89 V for $y = 0$ to 3.83 V for $y = 0.5$, which is ascribed to the formation of highly covalent vanadyl-type bonds (V=O)$^{2+}$ at the apex of the bioctahedra V$_2$O$_8$F$_{3-y}$O$_y$ that "continuously" replace the more ionic V–F bonds as y increases [9]. The extreme members of this family are Na$_3$(VO)$_2$(PO$_4$)$_2$F for $y = 1$ (often written as Na$_{1.5}$V^{IV}OPO$_4$F$_{0.5}$), and Na$_3$V$^{III}_2$(PO$_4$)$_2$F$_3$ (or Na$_{1.5}$V^{III}PO$_4$F$_{1.5}$) for $y = 0$. Since the ionic radii of V^{3+} and V^{4+} in the octahedral coordination are 0.64 Å and 0.58 Å, respectively, the cell volume increase would imply higher V^{3+} content in the samples.

The third of the sodium vanadium fluorophosphates, Na$_3$V$_2$(PO$_4$)$_2$F$_3$, was proposed by Barker et al. [12] in 2006. Its theoretical capacity of 192.4 mAh·g^{-1} corresponds to the extraction of three Na$^+$ ions from Na$_3$V$_2$(PO$_4$)$_2$F$_3$, however, a reversible extraction of only two Na$^+$ ions has been achieved in practice, resulting in a capacity of about 120 mAh·g^{-1}. As reported by Meins et al. [5], Na$_3$V$_2$(PO$_4$)$_2$F$_3$ has a tetragonal crystal structure, with the S.G. $P4_2/mnm$ and cell parameters $a = 9.047(2)$ Å and $c = 10.705(2)$ Å. In this structure, the V^{3+} ion is placed in the center of the VO$_4$F$_2$ octahedra, which are bridged together by one F$^-$ atom forming the V$_2$O$_8$F$_3$ bioctahedra, alternately connected by the PO$_4$ tetrahedra. This results in a stable 3D framework with large tunnels in the [110] and [1-10] directions. Recently, Bianchini et al. [13], using synchrotron X-ray powder diffraction, revealed a small but significant orthorhombic distortion in Na$_3$V$_2$(PO$_4$)$_2$F$_3$ ($b/a = 1.002$) and identified Na$_3$V$_2$(PO$_4$)$_2$F$_3$ in another orthorhombic crystal structure with the *Amam* S.G. This new structure preserves the framework but modifies the distribution of the Na$^+$ ions.

An overview of the literature data related to these three sodium fluorophosphates leads to some doubt about the real existence of these three different compounds, especially that of NaVPO$_4$F. This phase and its different polymorphs [4,14] have already been questioned by some authors [6]. Besides, the diffractograms of these phases are very similar, and their charge–discharge curves display two voltage plateau of close length at the same voltages.

The resulting composition of the material, its crystal structure and electrochemical performance, may be influenced by the synthetic method. As shown in Table 1, sodium vanadium fluorophosphates can be synthesized by various methods such as the solid-state reaction [3,6,8,9,12,13,15–17], solution-based carbothermic reduction [18,19], hydrothermal synthesis [5,10,11], sol–gel [4,20] and spray-drying synthesis [21]. The solid-state methods involve high-temperature treatment with a long period of mixing (up to 24 h) in low-energy mills. On the contrary, short-time high-energy mechanical activation significantly enhances solid-state reactions, thereby reducing the duration and temperature of the subsequent heat treatment and preparation of materials in a highly dispersed state [22].

Barker et al. first described the concept of a hybrid-ion battery, where a non-lithium-containing Na$_3$V$_2$(PO$_4$)$_2$F$_3$ cathode was used in conjunction with a conventional graphite anode material and a lithium electrolyte [23]. A hybrid-ion system composed of a traditional lithium-based non-aqueous electrolyte and a metallic lithium anode would be favored for the investigation of electrochemical properties of sodium-based materials, in order to develop theoretical basics, and to provide directions

for the construction of new high-energy rechargeable batteries. However, the mechanism of alkali ion insertion/deinsertion in these systems is not yet well understood [4,20,21,24–26].

We report here the energy-efficient mechanochemically-assisted solid-state synthesis of sodium vanadium fluorophosphates $Na_{1+y}VPO_4F_{1+y}$ ($0 \leq y \leq 0.75$) and the results of the comparative study of their crystal structure and electrochemistry in hybrid-ion cells.

Table 1. Synthetic methods for the preparation of $Na_3V_2(PO_4)_2F_3$.

Synthetic Method	Treatment Temperature	Treatment Time	Reference
Solid-state synthesis, CTR *	600–800 °C	8 h	Gover et al. [12]
Solid-state synthesis, CTR, MA **	750 °C	1.5 h	Shakoor et al. [16]
Solid-state synthesis, CTR, MA	800 °C	1 h	Bianchini et al. [13]
Solution-based solid-state synthesis	650 °C	8 h	Song et al. [18]
Hydrothermal reaction	180 °C	64 h	Le Meins et al. [5]
Sol–gel preparation	650 °C	8 h	Jiang et al. [20]
Spray drying	600 °C	2 h	Eshraghi et al. [21]
Solid-state synthesis, CTR, MA	650 °C	1 h	This work

* Carbothermal reduction; ** mechanical activation.

2. Results and Discussion

2.1. Crystal Structure and Morphology

Figure 1 shows the XRD patterns of the as-prepared products $Na_{1+y}VPO_4F_{1+y}$, with $y = 0$; 0.25; 0.5; 0.6 and 0.75. All samples were well-crystallized, however, only the sample with $y = 0.5$ was a single-phase material, which was assigned to $Na_3V_2(PO_4)_2F_3$ (hereinafter $Na_{1.5}VPO_4F_{1.5}$). The chemical composition of the sample with $y = 0.5$ determined by the Energy dispersive X-ray spectroscopy (EDX) analysis confirmed that the Na/V ratio was close to 1.5 (1.46). The other samples contained $Na_3V_2(PO_4)_2F_3$ as a main phase, and some impurities. For instance, $Na_3V_2(PO_4)_3$ [PDF 00-053-0018], VPO_4 [PDF 01-076-2023] or $NaVOPO_4$ [PDF 01-089-6316] were found as impurity phases in the samples with $y < 0.5$ (Table 2). When y exceeded 0.5, new weak reflections appeared, which could be assigned to other impurity phases such as Na_3VF_6 [PDF 00-029-1286], NaV_2O_5 [PDF 04-013-4702], Na_3PO_4 [PDF 04-015-4963].
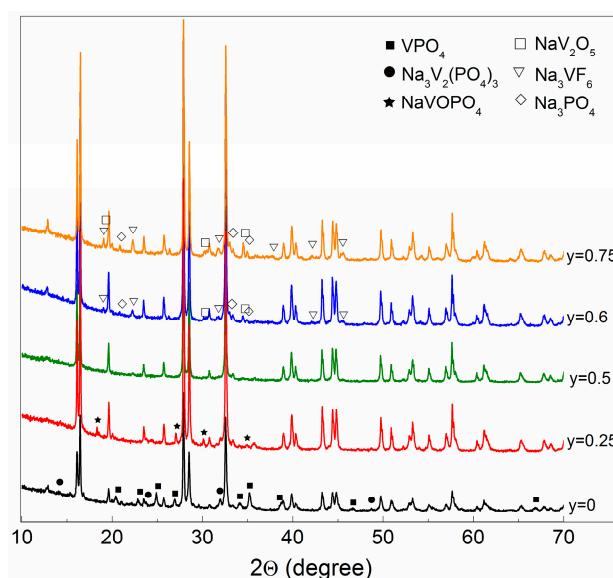

Figure 1. XRD patterns of the products obtained after subsequent annealing of the activated mixtures. $(1+y)NaF + VPO_4$ ($0 \leq y \leq 0.75$) at 650 °C in Ar flow.

Table 2. Phase composition of the as-prepared samples (%).

Sample (*y*)	Main Phase $Na_3V_2(PO_4)_2F_3$	Impurities		
0	80.6	$Na_3V_2(PO_4)_3$—4.6	VPO_4—14.8	-
0.25	92.5	-	-	$NaVOPO_4$—7.5
0.5	100	-	-	-
0.6	86.6	Na_3VF_6—2.9	NaV_2O_5—4.0	Na_3PO_4—6.5
0.75	78.9	Na_3VF_6—6.6	NaV_2O_5—4.8	Na_3PO_4—9.7

As mentioned above, two structural models ($P4_2/mnm$ and *Amam*) are known for $Na_3V_2(PO_4)_2F_3$, while the $I4/mmm$ S.G. is used for $NaVPO_4F$. Different compositions of sodium vanadium fluorophosphates $Na_3V_2O_{2y}(PO_4)_2F_{3-2y}$ described in the literature are summarized in Table 3, along with their space groups and the refined lattice parameters. It is seen that there is a strong dependence of the cell volume on the y value. For the samples with $y = 0$, the calculated volume is in the range of 876–879 Å^3, but when y approaches 1, it decreases to 865–868 Å^3 due to partial substitution of the F$^-$ ions by the O^{2-} ions and oxidation of the V^{3+} ions to the V^{4+} ions with lower ionic radius, thus indicating the formation of mixed-valence vanadium materials. In $Na_3V_2(PO_4)_2F_3$ with the $P4_2/mnm$ S.G.; the Na ions occupy the 8i sites, which have two different coordinates: two Na atoms are in the Na(1) sites and one Na atom is in the Na(2) site with the site occupancy factors (SOFs) of 1 and $\frac{1}{2}$, respectively. The *Amam* S.G. structure preserves the tetragonal framework but strongly impacts the sodium distribution in the planes. According to this model, the Na$^+$ ions are distributed in three crystallographic sites. Na(1) is placed in the center of a pyramidal site and its refined SOF is higher than 0.95, which means that this site is essentially fully occupied. Instead, the Na(2) and Na(3) sites cannot be simultaneously occupied, because of the vicinity of the Na ions ($d = 0.93$ Å). With respect to the surrounding environment, the Na(2) and Na(3) ions are not equivalent, since the first one occupies a pyramidal site, while the second one sits in a capped prism [13]. The structure of $NaVPO_4F$ was described by the authors [3] in the $I4/mmm$ S.G.; since it showed higher symmetry than $Na_3V_2(PO_4)_2F_3$.

Table 3. Lattice parameters of $Na_3V_2O_{2y}(PO_4)_2F_{3-2y}$ ($0 \leq y \leq 1$) described in the literature using different space groups.

Composition	S.G.	*a* = *b*, Å	*c*, Å	Volume, Å^3	Ref.
$NaVPO_4F$	$I4/mmm$	6.387(2)	10.734(3)	438.1	[3]
	$I4/mmm$	6.38	10.72	436.4	[4]
$Na_3V_2(PO_4)_2F_3$	$P4_2/mnm$	9.047(2)	10.705(2)	876.2(3)	[5]
	$P4_2/mnm$	9.0378(3)	10.7482(4)	877.94(6)	[12]
	$P4_2/mnm$	9.0358(2)	10.7403(4)	876.90(4)	[13]
	$P4_2/mnm$	9.04	10.74	877.69	[17]
	$P4_2/mnm$	9.05	10.74	876.9	[18]
	$P4_2/mnm$	9.04	10.73	877.0	[19]
$Na_3V_2(PO_4)_2F_3$	*Amam*	*a* = 9.0288(6) *b* = 9.0426(6)	10.7402(5)	876.88(9)	[13]
$Na_{1.5}VOPO_4F_{0.5}$	$I4/mmm$	6.37028(8)	10.6365(2)	431.63(1)	[6]
$Na_3V_2O_{2x}(PO_4)_2F_{3-2x}$	$P4_2/mnm$	9.02548–9.04499	10.63184–0.62113	866.1–869.0	[11]
$Na_{1.5}VO_{0.8}PO_4F_{0.7}$	$P4_2/mnm$	9.0332(1)	10.6297(2)	867.37(2)	[26]
$Na_{1.5}VOPO_4F_{0.5}$	$P4_2/mnm$	9.03051(2)	10.62002(3)	866.064	[7]

Figure 2 displays the XRD patterns of the $Na_{1+y}VPO_4F_{1+y}$ samples with $y = 0$ and $y = 0.5$ after Rietveld refinement using the $P4_2/mnm$ S.G., commonly employed to describe the structure of $Na_3V_2(PO_4)_2F_3$, and the *Amam* S.G., which characterizes an orthorhombic distortion [13] (see Materials and Methods). Both space groups appeared to be suitable for description of the structure of the $Na_3V_2(PO_4)_2F_3$ phase, though it is not surprising that the model with the low orthorhombic symmetry fit the experimental XRD patterns of the as-prepared samples better. When using the $I4/mmm$ S.G., we were unable to index the experimental

XRD pattern because of the presence of the 12.87, 23.5, 30.90, 35.97 2Θ reflections. The refined lattice parameters of the $Na_3V_2(PO_4)_2F_3$ main phase in all as-prepared samples are presented in Table 4. As can be seen, they coincided with each other and were close to the literature data [12]. Moreover, the calculated cell volumes pointed to the formation of the compounds without considerable substitution of the F^- ions by the O^{2-} ions, characteristic of the mixed valence phases $Na_3V_2O_{2x}(PO_4)_2F_{3-2y}$ ($0 \leq y \leq 1$), because the cell volume of the latter was significantly lower (see Table 3).

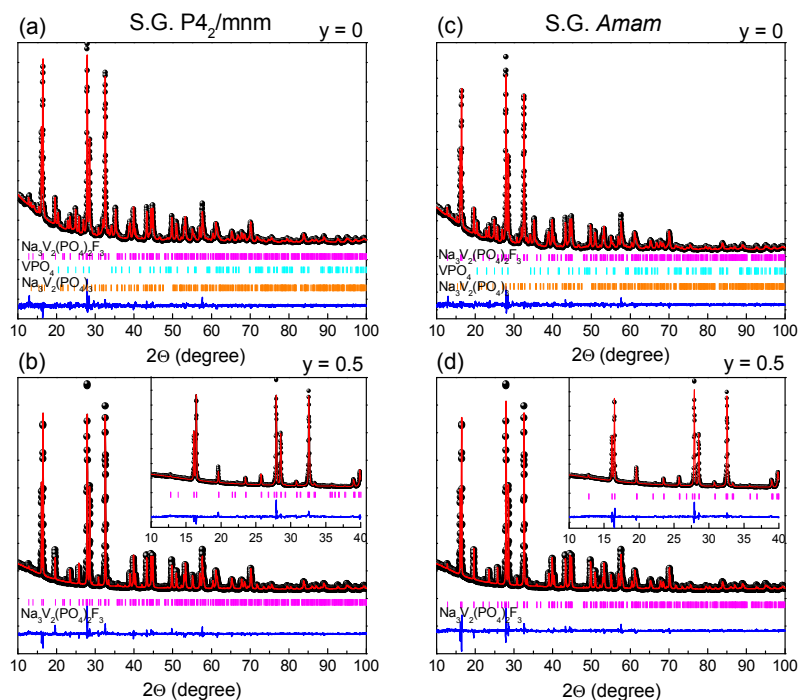**Figure 2.** XRD patterns of the $Na_{1+y}VPO_4F_{1+y}$ samples (**a**,**c**) with $y = 0$ and (**b**,**d**) $y = 0.5$ after Rietveld refinement (**a**,**b**) based on the tetragonal structure with S.G. $P4_2/mnm$ and (**c**,**d**) on the orthorhombic structure with S.G. *Amam*.

Table 4. Rietveld-refined lattice parameters of the as-prepared $Na_{1+y}VPO_4F_{1+y}$ ($y = 0$; 0.25; 0.5), based on the $P4_2/mnm$ and *Amam* space groups.

y	S.G.	$a = b$, Å	c, Å	V, Å³	GOF */R_{wp}
0.0	$P4_2/mnm$	9.0376(2)	10.7588(3)	878.77(5)	1.69/7.28
0.25	$P4_2/mnm$	9.0372(1)	10.7545(2)	878.32(3)	1.77/7.08
0.5	$P4_2/mnm$	9.0393(1)	10.7520(2)	878.54(2)	1.71/6.75
0.0	*Amam*	9.0298(5)/9.0465(5)	10.7595(3)	878.92(7)	1.64/6.61
0.25	*Amam*	9.0296(2)/9.0450(2)	10.7448(2)	878.37(4)	1.58/6.37
0.5	*Amam*	9.0323(2)/9.0467(2)	10.7523(1)	878.60(2)	1.44/5.73

* Goodness of fit (GOF).

The samples were also characterized by FTIR spectroscopy. Following from Figure 3, no significant differences were observed in the FTIR spectra of the as-prepared $Na_{1+y}VPO_4F_{1+y}$ samples. In all the spectra, the characteristic vibrations of the PO_4 groups (the T_d point group) were predominant [27]. In the spectral region of the internal modes of the PO_4 anion, symmetric ν_1 (a singlet) and asymmetric ν_3 (triply degenerated) stretching modes were located in the high-wavenumber region (900–1150 cm^{-1}) and were well separated from the bands due to asymmetric ν_4 (triply degenerated) and symmetric ν_2 (a doublet) bending vibrations that appeared in the low-wavenumber region (400–500 cm^{-1}). Therefore, the intense modes at 1140–1058 cm^{-1} and at 558 cm^{-1} on the experimental spectra corresponded to the stretching ν_3 and bending ν_4 vibrations of the P–O bonds in the PO_4 tetrahedron, respectively.

The higher intensity of the stretching mode at 944 cm^{-1} for the sample with $y = 0$ indicated the presence of a significant amount of VPO_4 impurity.
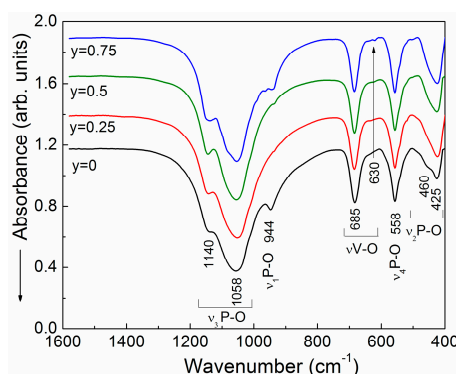

Figure 3. FTIR spectra of the $Na_{1+y}VPO_4F_{1+y}$ samples ($0 \leq y \leq 0.75$).

Although all the spectra were dominated by vibrational features due to the PO_4 ions, transition-metal ions also registered their presence in the middle region of 600–700 cm^{-1}. According to [6,28], the vibrations from the V^{3+}–O^{2-} bonds in the isolated VO_6 octahedra are evident at ~630 cm^{-1}. It is known that the signal corresponding to the characteristic short V=O vanadyl bond of the vanadium pentoxide is located at 1020 cm^{-1}, and this signal gradually shifts to lower wavenumbers during the reduction of V^{5+} to V^{4+} [29]. The occurrence of V^{5+} in the VO_6 octahedra were not observed, indicating that the V^{5+} ions were reduced to the V^{3+} ions in $Na_{1+y}VPO_4F_{1+y}$.

Morphological characterization of the $Na_{1+y}VPO_4F_{1+y}$ samples carried out by scanning electron microscopy (SEM) showed that the samples consisted of a mixture of irregular-shaped fine (primary) particles with an average particle size of about 100–200 nm, and large (secondary) micron-sized particles (from 0.5 μm to several micrometers) originated as a result of agglomeration of primary particles (Figure 4). The sample with $y = 0$ had slightly smaller particle size, probably due to formation of the multi-phase composition and simultaneous suppression of the crystal growth of each phase upon annealing of the activated mixtures.
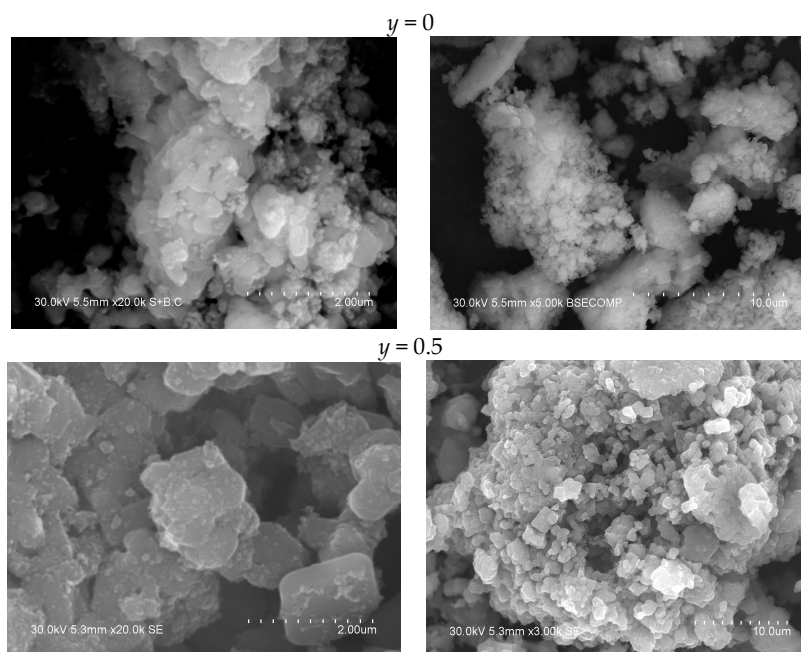

Figure 4. SEM images of the $Na_{1+y}VPO_4F_{1+y}$ samples with $y = 0$ and 0.5 with different magnification.

2.2. Electrochemistry

The electrochemical performance of the as-prepared samples was studied in hybrid Na/Li cells. Two methods were used. In the first case, the cathode material was placed in a lithium cell with a lithium anode, and the $LiPF_6$/EC+DMC (2:1) electrolyte (hereinafter Sample A), while in the second case, the cathode material was charged in a sodium cell with a sodium anode, and the $NaPF_6$/EC+DMC (2:1) electrolyte, then the cell was disassembled in a glove box, the cathode was washed with the DMC solution, and then put in a lithium cell (Sample B). Electrochemical testing was undertaken immediately following cell fabrication (typically within 10 min), thereby removing the possibility of any appreciable ion-exchange taking place between $Na_3V_2(PO_4)_2F_3$ and the electrolyte. Figure 5 shows the charge–discharge profiles and the dQ/dV vs. voltage plots of the first three cycles and the 20th cycle for the samples A with y = 0, 025 and 0.5 within the 3.0–4.6 V voltage range at the 0.1C rate. The charge–discharge curves consisted of two plateaus with an average voltage of 3.7–3.8 V and 4.3 V. It was seen that polarization was rather small for all three samples, indicating facile reversible alkali-ion (de)insertion reactions. The potential profiles of the 20th cycle exhibited a shape very similar to that of the first cycle. This indicates that the Li^+ ions replaced the Na^+ ions at the same crystallographic sites, and this replacement did not cause significant changes to the material structure.

Three oxidation peaks and three corresponding reduction peaks were observed on the dQ/dV vs. voltage plots: two close low-voltage peaks at 3.7–3.8 V, and one high-voltage peak at ~4.3 V. These values are very similar to those observed in Na cells [14,18], and the voltage difference was less than 0.3 V than expected. It was established that Na^+ ions at the Na2 sites are less stable than those at the Na1 sites, because they are farther shifted from the stable position [16]. Therefore, Na^+ ions at the Na2 sites would have a higher chemical potential than those at the Na1 sites, and thus, would be extracted at an earlier stage of charge and inserted at a later stage of discharge. According to [18], after extraction of the Na^+ ions from the Na2 sites, the remaining Na^+ ions are reorganized to the stable $Na_2V_2(PO_4)_2F_3$ configuration due to the short Na–Na distances between the ions occupying the Na1 sites.

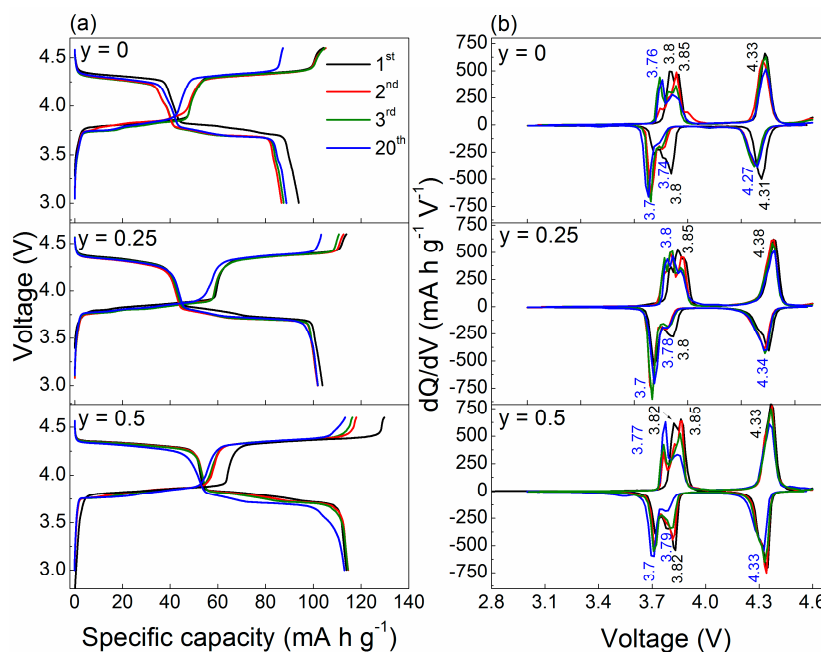**Figure 5.** (**a**) Galvanostatic cycling profiles and (**b**) the dQ/dV vs. voltage plots for the $Na_{1+y}VPO_4F_{1+y}$ (y = 0; 0.25; 0.5) samples in hybrid Na/Li cells. Cycling rate is C/10.

We noticed that during the few first cycles of $Na_{1+y}VPO_4F_{1+y}$ in hybrid cells, the relative intensity of the low-voltage redox peak at ~3.7 V gradually increased, presumably indicating an alternation

in the overall alkali ion insertion mechanism. Such an effect was first observed by Barker et al. [25] when studying the cycling of the $Li_{4/3}Ti_{5/3}O_4 || Na_3V_2(PO_4)_2F_3$ hybrid-ion cell. They suggested that during the first charge, the Na^+ ions are extracted from the fluorophosphate phase and entered into an electrolyte to create a mixed Li–Na electrolyte. The change in the intensity of the differential peak at ~3.7 V was explained as the transition from the predominant Na insertion mechanism at a cathode that is superimposed with Li in the lower voltage region, while the Na insertion dominates the higher voltage region, as can be seen from the maintenance of the intensity of the differential peak at ~4.3 V.

Ex situ XRD and EDX studies were performed to estimate the changes in structure and composition upon charge/discharge of $Na_{1+y}VPO_4F_{1+y}$ in a hybrid Na/Li cell, and the degree of the Na/Li electrochemical exchange. XRD patterns of the sample with $y = 0.5$ recorded at the end of the 12th charge and the 12th discharge in the Li cell are shown in Figure 6. On the XRD patterns of the sample at the end of the charge, some reflections of the initial phase disappeared, suggesting the occurrence of the reversible $P4_2/mnm \leftrightarrow I4/mmm$ transition, which was verified by the Rietveld refinement. The same structural transition was observed earlier during cycling of $Na_3V_2(PO_4)_2F_3$ in a Na cell [30]. The lattice parameters of the as-obtained products and the average sodium content per f.u. are shown in Table 5 in comparison with those presented in the literature [30]. It was seen that the refined lattice parameters were in a good agreement with those obtained in [30] for incompletely charged sodium vanadium fluorophosphate. According to the charge capacity and the XRD refinement, the final composition of the charged sample was ~$Na_{1.1}V_2(PO_4)_2F_3$, i.e.; it was not completely charged. Fully charged $Na_1V_2(PO_4)_2F_3$ was obtained by Bianchini et al. and indexed in the $Cmc2_1$ space group [30]. On the contrary, the XRD pattern of the sample, recorded at the end of the 12th discharge, showed the same set of reflections as the XRD pattern of the pristine sample. They were slightly shifted to larger angles, due to partial substitution of the Na ions for Li ions with lower ionic radius. The structure of the mixed Na/Li fluorophosphate was well refined with the $P4_2/mnm$ S.G., showing that the initial structure of $Na_3V_2(PO_4)_2F_3$ remained unchanged (Figure 6). The decreased occupancy of the Na sites testified that Li^+ ions replace the Na^+ ions at the same crystallographic sites. According to the EDX analysis, the Na/V ratio decreased from 1.46 for the pristine sample, to 1.26 for the mixed Na/Li fluorophosphate, thus resulting in the ~$Na_{2.52}Li_{0.48}V_2(PO_4)_2F_3$ composition, i.e.; only ~16% of Na ions were exchanged for Li ions during electrochemical cycling. This indicated that mixed Na/Li (de)intercalation occurs during cycling of $Na_3V_2(PO_4)_2F_3$ in a hybrid-ion cell, while the Na contribution is predominant. Sodium is never completely deinserted upon electrochemical cycling of $Na_3V_2(PO_4)_2F_3$. The immobile sodium therefore contributes to the structural stability of sodium vanadium fluorophosphates.

Table 5. Rietveld-refined lattice parameters and sodium content per formula unit for the sample with $y = 0.5$ charged and discharged in hybrid cells, compared to the literature data.

Sample	Stage	S.G.	$a = b$, Å	c, Å	V, Å^3	Na^+/f.u.	GOF/R_{wp}
$y = 0.5$	charge	$I4/mmm$	6.2496(2)	10.9568(7)	427.94(4)	0.54(2)	1.67/10.78
$y = 0.5$ (sample A)	discharge	$P4_2/mnm$	9.0251(3)	10.7524(6)	875.82(8)	1.30(2)	2.09/7.89
$y = 0.5$ (sample B)	discharge	$P4_2/mnm$	9.0175(12)	10.7000(19)	870.07(27)	0.82(6)	2.43/12.65
$Na_{1.3}(VPO_4)_2F_3$ [30]	charge	$I4/mmm$	6.2481(1)	10.9222(2)	426.39(1)	0.65	1.31(6)
$Na_{1.8}(VPO_4)_2F_3$ [30]	charge	$I4/mmm$	6.2800(1)	10.8493(3)	427.88(1)	0.9	1.85(7)

The mixed Na/Li ion intercalation resulted in the high capacity and excellent long-term stability of the hybrid electrochemical cells, as can be seen in Figure 7a. The highest initial discharge capacity (116 mAh·g^{-1}) was observed for the sample with $y = 0.5$. It corresponded to 90% of the theoretical material utilization, based on the assumption of participation by two alkali ions per f.u. of $Na_3V_2(PO_4)_2F_3$. For the other two samples with $y = 0$ and 0.25, the reversible specific capacity of 87 and 103 mAh·g^{-1}, respectively, was achieved. Such a difference in the values of specific capacity correlated with the amount of the electrochemically active $Na_3V_2(PO_4)_2F_3$ phase in these samples (Table 2).

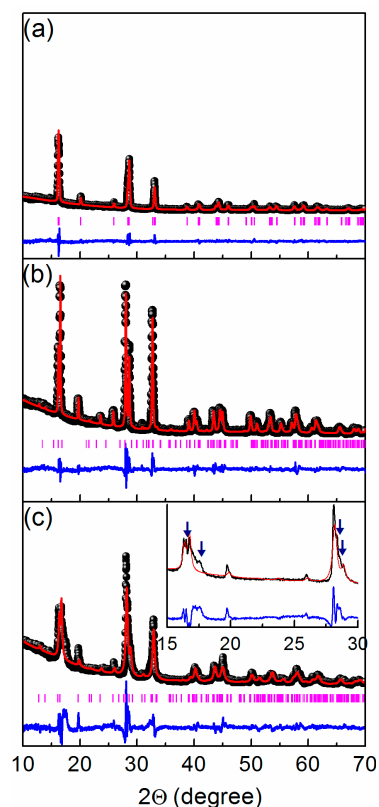**Figure 6.** Ex situ XRD pattern of the $Na_{1.5}VPO_4F_{1.5}$ (**a**,**b**) samples A and (**c**) B at the difference stages of charge–discharge in the Li cell after Rietveld refinement: (**a**) 12th charge ($I4/mmm$ S.G.); (**b**) 12th discharge ($P4_2/mnm$ S.G.), (**c**) seventh discharge ($P4_2/mnm$ S.G.). Arrows indicate the reflections of an unidentified phase.
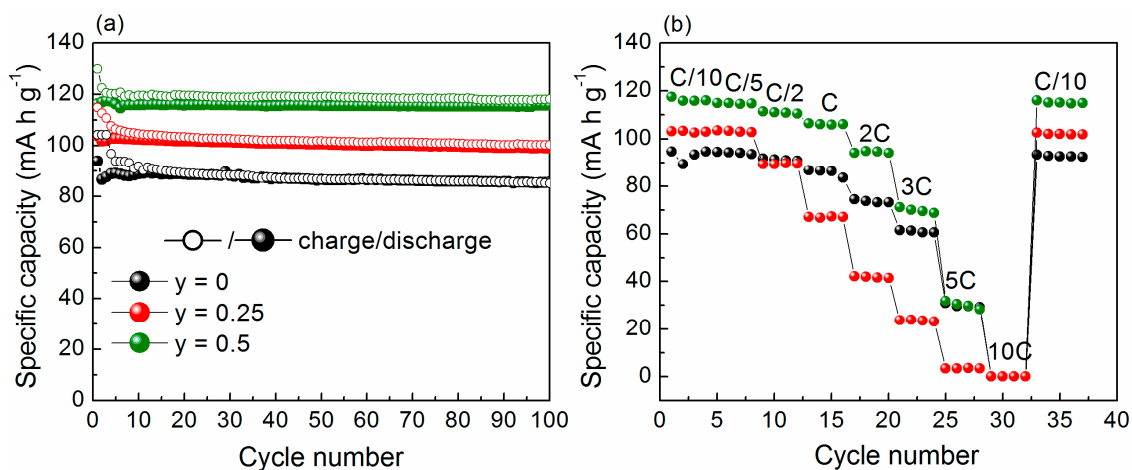

Figure 7. (**a**) The capacity vs. cycle number plots and (**b**) discharge capacity vs. cycling rate (C/10–10C) plots for $Na_{1+y}VPO_4F_{1+y}$ ($y = 0$; 0.25; 0.5).

According to Figure 7b, the as-prepared samples displayed a good high-rate performance. For instance, when the cycling rate increased from C/10 to 1C, the specific discharge capacity of the sample with $y = 0.5$ decreased only for 10%, from 116 to 106 mAh·g^{-1}. When the current density returned from 10C to C/10, the discharge capacity of the samples recovered to its initial value, proving high structural stability upon cycling.

When $Na_3V_2(PO_4)_2F_3$ was preliminarily charged to 4.6 V in the Na cell (sample B), ~1.9 Na ions per f.u. were extracted due to the oxidation of 1.9 V^{3+} ions to 1.9 V^{4+}. During further discharging in the Li cell, the electrolyte was free from Na ions. To compare the cycleability of samples A and B, we carried out the Galvanostatic intermittent titration technique (GITT) analysis. Figure 8a represents the charge–discharge curves obtained by GITT during the second cycle for these samples, illustrating voltage dependence on the Li content under load and rest. The cells were charged and discharged at a constant current C/10 (I_0 = 12.8 mA·g^{-1}) for an interval of 20 min followed by an open-circuit stand for 40 min to allow the cell voltage relaxing to its steady-state value. It was seen that the samples had different profiles: instead of two plateaus for sample A, only one plateau at lower voltage and a sloping charge–discharge curve at higher voltage was observed for sample B, presumably evidencing a single-phase mechanism of (de)insertion. However, the relaxation spikes in the latter case became longer, evidencing slower deintercalation reaction kinetics with larger polarization and slower equilibration. Moreover, according to the differential open circuit voltage (OCV) curves (Figure 8b), only one redox peak was clearly observed at 3.7 V, instead of two peaks at 3.7 and 3.8 V for sample A, while the occurrence and the position of the second peak at 4.3 V was preserved. Besides, additional low-intensive redox peaks were observed at ~4 V, evidencing a more complicated insertion mechanism. Based on the above-mentioned hypothesis, it can be assumed that the low-voltage cathode reaction that occurred in sample B was based mostly on the Li ions, while the high-voltage reaction was Na-based. According to the EDX analysis, the resulting Na/V ratio in sample B after its cycling in the Li cell was ~0.7, corresponding to the $Na_{1.4}Li_{1.6}V_2(PO_4)_2F_3$ composition. The XRD pattern of this mixed phase after Rietveld refinement is shown in Figure 6c. As can be seen, most reflections were similar to those observed for sample A (Figure 6b). A larger degree of the Li$^+$/Na$^+$ ion exchange was reflected in the significant reduction of the unit cell volume. However, some additional low-intensive reflections at 16.5, 17.5, 28.3, and 28.6 2Θ degree were identified, and could not be assigned to any known phases. Thus, though both samples were desodiated to a composition close to that at the first charge, regardless of whether it was in a Li or Na cell, their electrochemical behavior and the mechanism of the alkali ion insertion appeared to be different at the first discharge. The most probable reason for this is due to the composition of the electrolyte: the mixed electrolyte for sample A due to the deinsertion of the Na ions from sodium vanadium fluorophosphate upon the charge, or the mostly single Li electrolyte for sample B.
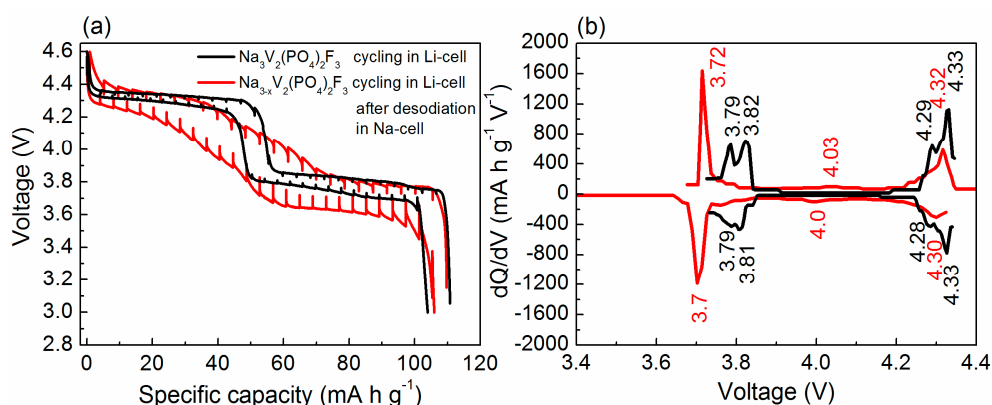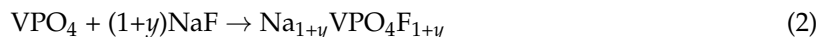

Figure 8. (**a**) GITT curves of the pristine $Na_{1.5}VPO_4F_{1.5}$ and electrochemically desodiated $Na_{1.5-x}VPO_4F_{1.5}$ in Li-cells, and (**b**) differential OCV curve vs. voltage plots.

3. Materials and Methods

A series of sodium-vanadium fluorophosphates $Na_{1+y}VPO_4F_{1+y}$ ($0 \leq y \leq 0.75$) were prepared by the two-step solid-state method, according to the following reactions using VPO_4 as an intermediate:

$$1/2V_2O_5 + NH_4H_2PO_4 + C \rightarrow VPO_4 + NH_3 + 3/2H_2O + CO, \quad (1)$$

$$VPO_4 + (1+y)NaF \rightarrow Na_{1+y}VPO_4F_{1+y} \tag{2}$$

The preliminary solid-state mechanical activation (MA) of both reagent mixtures was performed by means of a high-energy AGO-2 planetary mill (~900 rpm), with stainless jars and balls in Ar atmosphere for 5 min. The activated mixtures (1) and (2) were subsequently annealed in Ar flow for 2 h at 750 °C and 650 °C, respectively, and then slowly cooled to room temperature.

The XRD patterns of the as-prepared samples were recorded by a D8 Advance Bruker diffractometer (Bruker AXS GmbH, Karlsruhe, Germany) with a high-rate detector Lynx Eye, Cu $K\alpha_{1,2}$ radiation (λ_1 = 1.5406, λ_2 = 1.5445 Å), between 2θ = 10° and 100° with a step of 0.02° and an uptake time of 0.3 s. The structural refinement of the XRD data was carried out by the Rietveld method using TOPAS software [31]. First, we refined the structure of the single-phase sample (y = 0.5). The procedure was started with the refinement of the lattice parameters and followed by the atomic positions. The thermal displacement parameters for all atoms were refined just once, and then fixed at their final values; the thermal parameters for the atoms of the same elements were taken to be equal. Finally, the occupancy of the Na crystallographic sites was refined. The structural refinement of the main phase in the multi-phase samples was performed in a similar manner; all thermal parameters were kept fixed at the values extracted from the structural refinement of the single-phase sample. Particle size and morphology were investigated by SEM with a Hitachi S-3400 N scanning electron microscope (Hitachi High-Technologies Corporation, Tokyo, Japan). Chemical analysis of the synthesized materials was carried out by the energy-dispersive X-ray spectroscopy using an UltraDry EDX detector (Thermo Fischer Scientific Inc., Waltham, MA, USA). The FTIR spectra were recorded by means of a Tensor 27 spectrometer (Bruker Optik GmbH, Ettlingen, Germany) in the 400–4000cm^{-1} range (pellets with KBr).

The electrochemical properties of the as-prepared materials were studied in hybrid Na/Li cells. The composite cathode materials were fabricated by mixing 75 wt % active material with 20 wt % Super P (Timcal, Bodio, Switzerland), and a 5 wt % PVDF/NMP binder. The mixed slurry was then pasted on the aluminum foil to obtain the working electrodes. The total amount of carbon in the cathode mass was 20 wt %; mass loading was ~2–3 mg·cm^{-2} and an electrode diameter of 10 mm was used throughout. The Swagelok-type cells were assembled in an Ar filled glove box with Li metal as an anode, 1 M LiPF$_6$ solution in a mixture of ethylene carbonate (EC) and dimethyl carbonate (DMC) (2:1 by weight) as an electrolyte, and a glass fiber filter, Grade GF/C (GE Healthcare UK Ltd., Little Chalfont, UK) as a separator. The cycling was performed using a galvanostatic mode at the C/10–10C charge/discharge rates within the 3.0–4.6 V range. For ex situ experiments, the cathode mass was fabricated without a binder in a standard way: 80 wt % active material and 20 wt % Super P were ground thoroughly and then distributed uniformly at a current collector. In this case, the loading density was 20–21 mg·cm^{-2}. The cycling was stopped at the end of the charge or discharge, and a cell was disassembled inside an Ar glove box. The extracted electrodes were washed with DMC before being taken out of the box, dried in an argon atmosphere, and then studied by the XRD. For the GITT experiments, two methods of electrochemical measurement were used. For sample A, the initial cathode material was directly put in a lithium cell with a lithium anode and the LiPF$_6$/EC+DMC (2:1) electrolyte, while for sample B, the initial cathode material was charged in a sodium cell with a sodium anode and the NaPF$_6$/EC+DMC (2:1) electrolyte; the cell was then disassembled in a glove box, the cathode was carefully washed with the DMC solution to remove residues of the sodium electrolyte, and put in a lithium cell. GITT experiments were conducted, starting from the charge for sample A and from the discharge for sample B (after preliminary electrochemical desodiation). GITT was carried out with a current pulse of 12.8 mA·g^{-1} (0.1C) for 20 min followed by relaxation at an open circuit for 40 min at each step.

4. Conclusions

1. It has been shown that among sodium vanadium fluorophosphate compositions $Na_{1+y}VPO_4F_{1+y}$ ($0 \leq y \leq 0.75$) prepared by the mechanochemically assisted solid-state synthesis, the single-phase material $Na_{1.5}VPO_4F_{1.5}$ or $Na_3V_2(PO_4)_2F_3$ with a tetragonal structure (the $P4_2/mnm$ S.G.) was

formed only for $y = 0.5$. Samples with $y < 0.5$ and $y > 0.5$ possess different impurity phases. The compound with the $NaVPO_4F$ composition does not exist.

2. Sodium vanadium fluorophosphates $Na_{1+y}VPO_4F_{1+y}$ can be considered as multifunctional cathode materials for the fabrication of lithium-ion and sodium-ion high-energy batteries. The reversible discharge capacity of 116 mAh$\cdot$g^{-1} for $y = 0.5$, 103 mAh$\cdot$g^{-1} for $y = 0.25$ and 87 mAh$\cdot$g^{-1} for $y = 0$ was achieved. The decrease in the discharge capacity is in accordance with the amount of the electrochemically active phase $Na_3V_2(PO_4)_2F_3$ in the samples.

3. The ex situ XRD patterns confirm a reversible $P4_2/mnm \leftrightarrow I4/mmm$ transformation upon charging–discharging in a hybrid-ion cell, similar to the earlier observed transformation in Na-ion cells.

4. The structural study of charged and discharged samples and the analysis of the differential capacity curves indicated a negligible Na/Li electrochemical exchange (~16%) and a predominantly sodium-based cathode reaction in the hybrid-ion cell. This is significantly lower than the ~50% exchange observed for other Na-based cathodes, such as Na_2FePO_4F [32] and $Na_2FeP_2O_7$ [33] when cycled in hybrid-ion cells, showing that the properties of hybrid-ion batteries can be varied based on the alkali-ion selectivity of electrode materials. To increase the degree of the Na/Li electrochemical exchange in $Na_3V_2(PO_4)_2F_3$, it first needs to be desodiated in a Na cell, and then cycled in a Li cell with the electrolyte enriched with Li ions.

5. After cycling in hybrid-ion cells, $Na_3V_2(PO_4)_2F_3$ showed nice cycleability and high-rate performance, presumably due to operating in the mixed Na/Li electrolyte. Thus, the hybrid-ion approach may open possibilities for many new active materials and material combinations with enhanced electrochemical performance. This approach provides an opportunity for sodium cathode materials to be used without the requirement for ion Na/Li exchange prior to cell fabrication. Since in hybrid-ion systems all anodic charge carriers originate from the electrolyte, this may limit their use in high-energy applications, where relatively thick electrodes are used in combination with thin electrolytes. However, in high power applications, this may not represent a major drawback, since thinner electrodes and thicker electrolytes are commonly used.

Author Contributions: Nina V. Kosova conceived and designed the experiments; Daria O. Rezepova performed the experiments; both authors participated in the analysis of the experimental data and in writing the paper.

Conflicts of Interest: The authors declare no conflict of interest.

References

1. Yabuuchi, N.; Kubota, K.; Dahbi, M.; Komaba, S. Research development on sodium-ion batteries. *Chem. Rev.* **2014**, *114*, 11636. [CrossRef] [PubMed]

2. Masquelier, C.; Croguennec, L. Polyanionic (phosphates, silicates, sulfates) frameworks as electrode materials for rechargeable Li (or Na) batteries. *Chem. Rev.* **2013**, *113*, 6552–6591. [CrossRef] [PubMed]

3. Barker, J.; Saidi, M.Y.; Swoyer, J.L. A sodium-ion cell based on the fluorophosphate compound $NaVPO_4F$. *Electrochem. Solid State Lett.* **2003**, *6*, A1–A4. [CrossRef]

4. Zhao, J.; He, J.; Ding, X.; Zhou, J.; Ma, Y.; Wu, S.; Huang, R. A novel sol–gel synthesis route to $NaVPO_4F$ as cathode material for hybrid lithium ion batteries. *J. Power Sources* **2010**, *195*, 6854–6859. [CrossRef]

5. Le Meins, J.-M.; Crosnier-Lopez, M.-P.; Hemon-Ribaud, A.; Courbion, G. Phase transitions in the $Na_3M_2(PO_4)_2F_3$ family (M = Al^{3+}, V^{3+}, Cr^{3+}, Fe^{3+}, Ga^{3+}): Synthesis, thermal, structural, and magnetic studies. *J. Solid State Chem.* **1999**, *148*, 260–277. [CrossRef]

6. Sauvage, F.; Quarez, E.; Tarascon, J.M.; Baudrin, E. Crystal structure and electrochemical properties vs. Na$^+$ of the sodium fluorophosphate $Na_{1.5}VOPO_4F_{0.5}$. *Solid State Sci.* **2006**, *8*, 1215–1221. [CrossRef]

7. Tsirlin, A.A.; Nath, R.; Abakumov, A.M.; Furukawa, Y.; Johnston, D.C.; Hemmida, M.; Krug von Nidda, H.-A.; Loidl, A.; Geibel, C.; Rosner, H. Phase separation and frustrated square lattice magnetism of $Na_{1.5}VOPO_4F_{0.5}$. *Phys. Rev. B* **2011**, *84*, 014429. [CrossRef]

8. Park, Y.U.; Seo, D.H.; Kim, H.; Kim, J.; Lee, S.; Kim, B.; Kang, K. A family of high-performance cathode materials for Na-ion batteries, $Na_3(VO_{1-x}PO_4)_2F_{1+2x}(0 \le x \le 1)$: Combined first-principles and experimental study. *Adv. Funct. Mater.* **2014**, *24*, 4603–4614. [CrossRef]

9. Broux, T.; Bamine, T.; Fauth, F.; Simonelli, L.; Olszewski, W.; Marini, C.; Menetrier, M.; Carlier, D.; Masquelier, C. Strong impact of the oxygen content in $Na_3V_2(PO_4)_2F_{3-y}O_y$ $(0 \le y \le 0.5)$ on its structural and electrochemical properties. *Chem. Mater.* **2016**, *28*, 7683–7692. [CrossRef]

10. Serras, P.; Palomares, V.; Goni, A.; Kubiak, P.; Rojo, T. Electrochemical performance of mixed valence $Na_3V_2O_{2x}(PO_4)_2F_{3-2x}$/C as cathode for sodium-ion batteries. *J. Power Sources* **2013**, *241*, 56–60. [CrossRef]

11. Serras, P.; Palomares, V.; Goni, A.; Gil de Muro, I.; Kubiak, P.; Lezama, L.; Rojo, T. High voltage cathode materials for Na-ion batteries of general formula $Na_3V_2O_{2x}(PO_4)_2F_{3-2x}$. *J. Mater. Chem.* **2012**, *22*, 22301–22308. [CrossRef]

12. Gover, R.K.B.; Bryan, A.; Burns, P.; Barker, J. The electrochemical insertion properties of sodium vanadium fluorophosphate, $Na_3V_2(PO_4)_2F_3$. *Solid State Ion.* **2006**, *177*, 1495–1500. [CrossRef]

13. Bianchini, M.; Brisset, N.; Fauth, F.; Weill, F.; Elkaim, E.; Suard, E.; Masquelier, C.; Croguennec, L. $Na_3V_2(PO_4)_2F_3$ revisited: A high-resolution diffraction study. *Chem. Mater.* **2014**, *26*, 4238–4247. [CrossRef]

14. Zhuo, H.; Wang, X.; Tang, A.; Liu, Z.; Gamboa, S.; Sebastian, P.J. The preparation of $NaV_{1-x}Cr_xPO_4F$ cathode materials for sodium-ion battery. *J. Power Sources* **2006**, *160*, 698–703. [CrossRef]

15. Lu, Y.; Zhang, S.; Li, Y.; Xue, L.; Xu, G.; Zhang, X. Preparation and characterization of carbon-coated $NaVPO_4F$ as cathode material for rechargeable sodium-ion batteries. *J. Power Sources* **2014**, *247*, 770–777. [CrossRef]

16. Shakoor, R.A.; Seo, D.-H.; Kim, H.; Park, Y.-U.; Kim, J.; Kim, S.-W.; Gwon, H.; Lee, S.; Kang, K. A combined first principles and experimental study on $Na_3V_2(PO_4)_2F_3$ for rechargeable Na batteries. *J. Mater. Chem.* **2012**, *22*, 20535–20541. [CrossRef]

17. Chihara, K.; Kitajou, A.; Gocheva, I.D.; Okada, S.; Yamaki, J. Cathode properties of $Na_3M_2(PO_4)_2F_3$ [M = Ti, Fe, V] for sodium-ion batteries. *J. Power Sources* **2013**, *227*, 80–85. [CrossRef]

18. Song, W.; Cao, X.; Wu, Z.; Chen, J.; Zhu, Y.; Hou, H.; Lan, Q.; Ji, X. Investigation of the sodium ion pathway and cathode behavior in $Na_3V_2(PO_4)_2F_3$ combined via a first principles calculation. *Langmuir* **2014**, *30*, 12438–12466. [CrossRef] [PubMed]

19. Liu, Z.; Hu, Y.-Y.; Dunstan, M.T.; Huo, H.; Hao, X.; Zou, H.; Zhong, G.; Yang, Y.; Grey, C.P. Local structure and dynamics in the Na ion battery positive electrode material $Na_3V_2(PO_4)_2F_3$. *Chem. Mater.* **2014**, *26*, 2513–2521. [CrossRef]

20. Jiang, T.; Chen, G.; Li, A.; Wang, C.; Wei, Y. Sol–gel preparation and electrochemical properties of $Na_3V_2(PO_4)_2F_3$/C composite cathode material for lithium ion batteries. *J. Alloys Compd.* **2009**, *478*, 604–607. [CrossRef]

21. Eshraghi, N.; Caes, S.; Mahmoud, A.; Cloots, R.; Vertruyen, B.; Boschini, F. Sodium vanadium (III) fluorophosphate/carbon nanotubes composite (NVPF/CNT) prepared by spray-drying: Good electrochemical performance thanks to well-dispersed CNT network within NVPF particles. *Electrochim. Acta* **2017**, *228*, 319–324. [CrossRef]

22. Kosova, N. Mechanochemical reactions and processing of nanostructured electrode materials for lithium-ion batteries. *Mater. Today Proc.* **2016**, *3*, 391–395. [CrossRef]

23. Barker, J.; Gover, R.K.B.; Burns, P.; Bryan, A.J. Hybrid-ion. A lithium-ion cell based on a sodium insertion material. *Electrochem. Solid State Lett.* **2006**, *9*, A190–A192. [CrossRef]

24. Song, W.; Liu, S. A sodium vanadium three-fluorophosphate cathode for rechargeable batteries synthesized by carbothermal reduction. *Solid State Sci.* **2013**, *15*, 1–6. [CrossRef]

25. Barker, J.; Cover, R.; Burns, P.; Bryan, A.J. $Li_{4/3}Ti_{5/3}O_4 \mid\mid Na_3V_2(PO_4)_2F_3$: An example of a hybrid-ion cell using a non-graphitic anode. *J. Electrochem. Soc.* **2007**, *154*, A882–A887. [CrossRef]

26. Park, Y.-U.; Seo, D.-H.; Kim, B.; Hong, K.-P.; Kim, H.; Lee, S.; Shakoor, R.A.; Miyasaka, K.; Tarascon, J.-M.; Kang, K. Tailoring a fluorophosphate as a novel 4 V cathode for lithium-ion batteries. *Sci. Rep.* **2012**, *704*, 1–7. [CrossRef] [PubMed]

27. Ait Salah, A.; Jozwiak, P.; Garbarczyk, J.; Benkhouja, K.; Zaghib, K.; Gendron, F.; Julien, C.M. Local structure and redox energies of lithium phosphates with olivine- and Nasicon-like structures. *J. Power Sources* **2005**, *140*, 370–375. [CrossRef]

28. Kosova, N.V.; Devyatkina, E.T.; Slobodyuk, A.B.; Gutakovskii, A.K. LiVPO$_4$F/Li$_3$V$_2$(PO$_4$)$_3$ nanostructured composite cathode materials prepared via mechanochemical way. *J. Solid State Electrochem.* **2014**, *18*, 1389–1399. [CrossRef]

29. Kera, Y. Infrared study of alkali tri- and hexavanadates as formed from their melts. *J. Solid State Chem.* **1984**, *51*, 205–211. [CrossRef]

30. Bianchini, M.; Fauth, F.; Brisset, N.; Weill, F.; Suard, E.; Masquelier, C.; Croguennec, L. A comprehensive investigation of the Na$_3$V$_2$(PO$_4$)$_2$F$_3$–NaV$_2$(PO$_4$)$_2$F$_3$ system by operando high resolution synchrotron X-ray diffraction. *Chem. Mater.* **2015**, *27*, 3009–3020. [CrossRef]

31. Cheary, R.W.; Coelho, A.A. A fundamental parameters approach to X-ray line-profile fitting. *J. Appl. Cryst.* **1992**, *25*, 109–121. [CrossRef]

32. Kosova, N.V.; Podugolnikov, V.R.; Devyatkina, E.T.; Slobodyuk, A.B. Structure and electrochemictry of NaFePO$_4$ and Na$_2$FePO$_4$F cathode materials prepared via mechanochemical route. *Mater. Res. Bull.* **2014**, *60*, 849–857. [CrossRef]

33. Kosova, N.V.; Rezepova, D.O.; Petrov, S.A.; Slobodyuk, A.B. Elelctrochemical and chemical Na$^+$/Li$^+$ ion exchange in Na-based cathode materials: Na$_{1.56}$Fe$_{1.22}$P$_2$O$_7$ and Na$_3$V$_2$(PO$_4$)$_2$F$_3$. *J. Electrochem. Soc.* **2017**, *164*, A6192–A6200. [CrossRef]